Chem. Senses 30: 615–626, 2005
doi:10.1093/chemse/bji055
Advance Access publication September 1, 2005

Analysis of Training-Induced Changes in Ethyl Acetate Odor Maps Using a New Computational Tool to Map the Glomerular Layer of the Olfactory Bulb

Ernesto Salcedo[1,2,3], Chunbo Zhang[4,5], Eugene Kronberg[1,2,3] and Diego Restrepo[1,2,3]

[1]Department of Cell and Developmental Biology, University of Colorado School of Medicine, Mail Stop 8108 PO Box 6511, Aurora, CO 80045, USA, [2]Neuroscience Program, University of Colorado School of Medicine, Mail Stop 8108 PO Box 6511, Aurora, CO 80045, USA, [3]Rocky Mountain Taste and Smell Center, University of Colorado School of Medicine, Mail Stop 8108 PO Box 6511, Aurora, CO 80045, USA, [4]Biology Division, BCPS, Illinois Institute of Technology, Chicago, IL 60616, USA and [5]Center for Integrative Neuroscience and Neuroengineering, Illinois Institute of Technology, Chicago, IL 60616, USA

Correspondence to be sent to: Ernesto Salcedo, Department of Cell and Developmental Biology, University of Colorado at Denver and Health Sciences Center at Fitzsimons, Mail Stop 8108 PO Box 6511, Aurora, CO 80045, USA. e-mail: ernesto.salcedo@uchsc.edu

Abstract

Odor quality is thought to be encoded by the activation of partially overlapping subsets of glomeruli in the olfactory bulb (odor maps). Mouse genetic studies have demonstrated that olfactory sensory neurons (OSNs) expressing a particular olfactory receptor target their axons to a few individual glomeruli in the bulb. While the specific targeting of OSN axons provides a molecular underpinning for the odor maps, much remains to be understood about the relationship between the functional and molecular maps. In this article, we ask the question whether intensive training of mice in a go/no-go operant conditioning odor discrimination task affects odor maps measured by determining *c-fos* up-regulation in periglomerular cells. Data analysis is performed using a newly developed suite of computational tools designed to systematically map functional and molecular features of glomeruli in the adult mouse olfactory bulb. This suite provides the necessary tools to process high-resolution digital images, map labeled glomeruli, visualize odor maps, and facilitate statistical analysis of patterns of identified glomeruli in the olfactory bulb. The software generates odor maps (density plots) based on glomerular activity, density, or area. We find that training up-regulates the number of glomeruli that become *c-fos* positive after stimulation with ethyl acetate.

Key words: *c-fos*, glomerulus, go/no-go operant conditioning, neuroinformatics, odor map, olfactory bulb

Introduction

At the cellular and molecular level, the sense of smell is a complex task of odorant detection and signal processing that entails the discrimination of thousands of volatile molecules with diverse chemical structures. The mammalian olfactory system has evolved to handle this complex problem by expressing in the olfactory epithelium a large array of olfactory sensory neurons (OSNs), each tuned to a subset of odorants with shared structural features (Buck, 2000). OSNs with identical chemical sensitivities are distributed quasirandomly within circumscribed expression zones in the olfactory epithelium. These OSNs extend their single axon into a few discrete, spherical neuropil structures (glomeruli) in the glomerular layer of the main olfactory bulb (MOB) (Shepherd *et al.*, 2004). Thus, each glomerulus contains the axons from several thousand OSNs, which, regardless of the location in the soma of the epithelium, all express the same odorant receptor (OR) (Vassar *et al.*, 1993; Ressler *et al.*, 1994; Mombaerts *et al.*, 1996). OSNs expressing the same OR typically target two symmetric mirror areas in each olfactory bulb. In this fashion, the responses of OSNs distributed throughout the olfactory epithelium are organized into a spatiotemporal pattern of glomerular activation at the first synaptic neuropil in the MOB.

Many studies have shown region-specific increases in activity in the glomerular layer of the bulb in response to odor exposure (Sharp *et al.*, 1977; Royet *et al.*, 1987; Friedrich and Korsching, 1998; Rubin and Katz, 1999; Nagao *et al.*, 2000; Johnson and Leon, 2000b; Wachowiak and Cohen, 2001; Schaefer *et al.*, 2001b). Moreover, the response of glomeruli in the MOB appears to be arranged chemotopically

(Johnson *et al.*, 1999; Uchida *et al.*, 2000; Johnson and Leon, 2000a). These independent lines of evidence support the hypothesis that the glomerular arrangement in the olfactory bulb provides an anatomical foundation for the encoding of odorant quality and intensity. Indeed, the position of individual glomeruli, while not invariant (Strotmann *et al.*, 2000; Schaefer *et al.*, 2001a), can be determined within a 95% confidence interval (Schaefer *et al.*, 2001a). Thus, the position of individual glomeruli and the overall glomerular synaptic activity in the MOB serve as important metrics in the investigation of olfactory function and odor coding.

Methods used to detect glomerular activity throughout the olfactory bulb include functional magnetic resonance imaging (fMRI), 2-deoxyglucose (2-DG) autoradiography, and the *in situ* detection of immediate early genes (IEG) expression such as Fos or Zif268. fMRI, which is performed in anesthetized animals, tracks changes in spin relaxation properties of water molecules thought to reflect activity-dependent changes in blood flow (Xu *et al.*, 2000b, Xu *et al.*, 2005). The other two methods require the sectioning of harvested olfactory bulbs from sacrificed animals and thus lack a temporal aspect to the pattern. 2-DG autoradiography, which tracks changes in cellular metabolism, labels the intensity of cellular metabolism markers. The *in situ* detection of IEG expression, which tracks odor-induced changes in the expression pattern for mRNA or protein in juxtaglomerular cells, can be used to label the individual locations of activated glomeruli at the resolution of a single glomerulus (Sharp *et al.*, 1977; Guthrie *et al.*, 1993; Sallaz and Jourdan, 1993; Johnson *et al.*, 1999; Johnson and Leon, 2000b; Inaki *et al.*, 2002). Ultimately, all these methods generate a comprehensive spatial pattern of glomerular activity elicited from a particular odor that is typically referred to as an odor map (Xu *et al.*, 2000a).

In this article, we study the effect of intensive training of mice in a go/no-go operant conditioning odor detection task on ethyl acetate (EA)–elicited odor maps measured through the increased transcription of the IEG *c-fos* in periglomerular cells. Go/no-go operant conditioning has been used extensively to study the detection and discrimination of odors by adult rodents (Slotnick and Bodyak, 2002). This olfactory learning paradigm is particularly useful in the study of olfactory deficits in mice (Munger *et al.*, 2001; Lin *et al.*, 2004; Vedin *et al.*, 2004) and has the advantage that it can be used in a computer-controlled olfactometer that can accurately deliver the stimulus and reinforcement (Bodyak and Slotnick, 1999). While operant conditioning is increasingly being used in various studies, little is known about the plastic changes that presumably take place in the olfactory bulb during operant conditioning in adult mice. To better understand these mechanisms, we examined the changes in odor-induced *c-fos* expression patterns elicited by operant conditioning training in the mouse MOB. Changes in the induction of *c-fos* in the juxtaglomerular and granule cells of the MOB have been observed in early preference learning in rats (Johnson *et al.*, 1995). In addition, familiarization with an odor has been shown to change the extent of odor-elicited *c-fos* induction in granule cells in adult rats (Montag-Sallaz and Buonviso, 2002). For our study, we examined the distribution of odor-induced *c-fos* mRNA up-regulation in juxtaglomerular cells throughout the entire MOB after operant conditioning and compared them to odor maps in naïve, mice.

To accurately compare the odor maps between animals, we used a new suite of computational tools developed to map activity patterns detected by markers such as 2-DG or IEGs. Our software can also map the location of individual glomeruli labeled by a genetic marker such as β-galactosidase or green fluorescent protein (GFP) (Mombaerts *et al.*, 1996) to within biological variation. We designed this software suite not only to implement our mapping technique (Schaefer *et al.*, 2001a), but also to be flexible enough to accommodate other mapping methods. Odor maps can be displayed individually as a two-dimensional (2-D) or three-dimensional (3-D) representation, or in the case of the (3-D) representations, as a combined odor map. In a combined representation, molecularly tagged glomeruli can serve as fiduciary points relating odor activity maps to the underlying probabilistic anatomical map of OSN axon targeting the glomerular layer of the bulb.

Materials and methods

Operant conditioning

FVB mice approximately 3 months of age were water restricted and divided into two groups, EA trained (trained) and naïve. Mice were trained using an operant conditioning go/no-go paradigm in a Bodyak–Slotnick olfactometer as described in Bodyak and Slotnick (1999). Briefly, water-deprived mice were trained using water reinforcement to sample a 2.0-s stimulus presentation. The mice were trained to respond to the presence of an odor (S+ stimulus) by licking a water delivery tube and refrained from responding in the presence of no odor (S− stimulus). Trained mice were given intensive operant conditioning training by taking them through a training schedule designed to allow determination of detection thresholds by the descending method of limits. The S+ stimulus was EA diluted in mineral oil, and the S− stimulus was mineral oil. Subsequently, lower EA odor concentrations (a 1/40 dilution of air equilibrated with 10^{-2}, $10^{-2.3}$, 10^{-3}, 10^{-4}, 10^{-5}, and 10^{-6}% EA in mineral oil) were tested in each of the go/no-go sessions. Each session was terminated when a mouse reached criterion (when it responded 85% correct or better on three consecutive blocks of 20 trials). Whenever possible, two sessions were run in each day. Attempts to run more than two sessions per day were unsuccessful because the mice would not behave in the olfactometer in the third session. Testing was stopped when the mouse responded below 85% in six blocks. A session where the mouse was asked to detect the difference between two vials containing mineral oil (no EA added) was run to ensure that the mice

were not cueing on nonchemosensory stimuli. During this period, naïve mice underwent water restriction by receiving the same amount of water as the trained mice (1 ml daily). Both groups of mice then received free access to water for a week before assessment of odor-induced *c-fos* up-regulation.

Detection of *c-fos*–positive glomeruli

One week after training, mice were exposed to either air (control) or a moderately strong concentration of EA (greater than 99% purity, Aldrich Chemical Company, St. Louis, MO) mixed in mineral oil to a 0.01% concentration. Notice that, in contrast to the behavioral experiments above, where there is a further 1/40 dilution with air, there is no further dilution in this experiment. After odor exposure, the mice were immediately sacrificed and perfused with 4% paraformaldehyde. The olfactory bulbs were then harvested and cryopreserved. Transverse serial sections (18 μm) of the olfactory bulbs were cut in a plane perpendicular to the olfactory tract. Antisense cRNA transcribed from a mouse recombinant cDNA clone corresponding to positions 1842–1944 and 2061–2493 of the mouse *c-fos* gene (MUSFOS) was used to determine the expression of *c-fos* mRNA in the juxtaglomerular cells (periglomerular and external tufted cells) surrounding glomeruli. *In situ* hybridization was performed as detailed in Schaefer *et al.* (2001b). Glomeruli were scored as positive when an arc of labeled juxtaglomerular cells spanning either 180° in any orientation or two 90° arcs spanning any region were identified.

Mapping technique

Our mapping technique implements the coordinate system and mapping procedure introduced in our previous studies (Schaefer *et al.*, 2001a,b). Using this technique, we map the cylindrical coordinates of glomeruli onto the digital images of transverse cryosections of murine olfactory bulbs, which must be sectioned perpendicular to the lateral olfactory tract (Figure 1A, line L). The cylindrical coordinates are the rostro–caudal distances measured from the anterior to the posterior region of the bulb (Figure 1B), the angle around a section (Figure 1C, angle between dashed line and origin line), and the radius (Figure 1C, dashed line) from the origin within each section. We use anatomical landmarks within the bulb to determine the origins from which these coordinates are measured. The rostral landmark, which defines the origin of the rostro–caudal axis, contains the first clear mitral cell and external plexiform layers (Johnson *et al.*, 1999) (Figure 1B, i). Distances posterior to this landmark are indexed as positive numbers. The accessory olfactory bulb (AOB) landmark contains the first, clear accessory bulb (AOB) granule and glomerular layer (Figure 1B, iii). The distance from the origin landmark to the AOB landmark is used to determine consistency in the cutting angle between mice. Deviation from cuts perpendicular to the L plane (e.g., cutting perpendicular to the dorsal surface of the brain—the C plane in Figure 1A) results in a variation in this distance.

To determine the rostro–caudal distance for a glomerulus, we record the distance caudal to the rostral landmark for each transverse section of interest by counting the number of sections from the rostral origin landmark to the transverse section containing the glomerulus. We then multiply that number by the thickness of a section (typically 18 μm). At that point, for the section containing the glomerulus, we determine the origin and orientation of the 0°–180° axis for the cylindrical coordinate system by drawing a straight line from the dorsal to the ventral mitral cell layers (Figure 1B, i–iv—black lines). The definition of this origin line differs depending on the rostro–caudal location of the section as the anatomical landmarks used to determine the origin and its orientation change along this dimension. For each section rostral to the AOB landmark, we draw a straight line that bisects the lower two-thirds of the subependymal zone (SEZ), orienting the 0°–180° axis along the dorsoventral axis of the section (Figure 1B, i and ii). We set the point of origin at one-third the distance from the dorsal to the ventral mitral cell layers. Thus, in our coordinate system, 0° corresponds approximately to the dorsal region of the bulb, while 90°, 180°, and 270° correspond to the lateral, ventral, and medial regions of the bulb, respectively (Figure 1C). For sections cut at or caudal to the AOB landmark, we draw a line from the granular cusp of the AOB to the ventral mitral cell layer, maintaining an orientation that bisects the SEZ. In these sections, we set the origin immediately dorsal to the granule cusp of the MOB (Figure 1B, iii and iv). Once we have set a point of origin, we trace the perimeter at the boundary between the external plexiform layer and the glomerular layer (Figure 1C), which allows us to convert angle coordinates to perimeter measurements and vice versa. Next, we trace the outline of any glomeruli of interest and record the coordinates. For example, the small circle drawn on the cryosection in Figure 1C is a glomerulus measured to be at 58° using our coordinate system. As this section is the 35th section from the rostral landmark in a bulb sectioned at 36 μm, we record its rostro–caudal distance as 1,260 μm. The location of the glomerulus in a map of angle versus rostro–caudal distance is shown in Figure 1D. In this plot, the index for the rostral landmark is set to one.

Mapping software

Our mapping software includes two programs for mapping glomerular location: (1) a Java plugin (Glomerular Analysis) for the open-source image processing program, ImageJ (http://rsb.info.nih.gov/ij/) and (2) a more comprehensive and flexible toolbox (GLOM•MAP *OBS*) for the cross-platform MATLAB environment (The MathWorks, Inc., Natick, MA). Using either of these two software packages, a user can open high-resolution digital images of olfactory bulbs and map the location of glomeruli across multiple sections. These maps can then be loaded into our MATLAB statistical analysis toolbox, GLOM•MAP *GDB*, which is

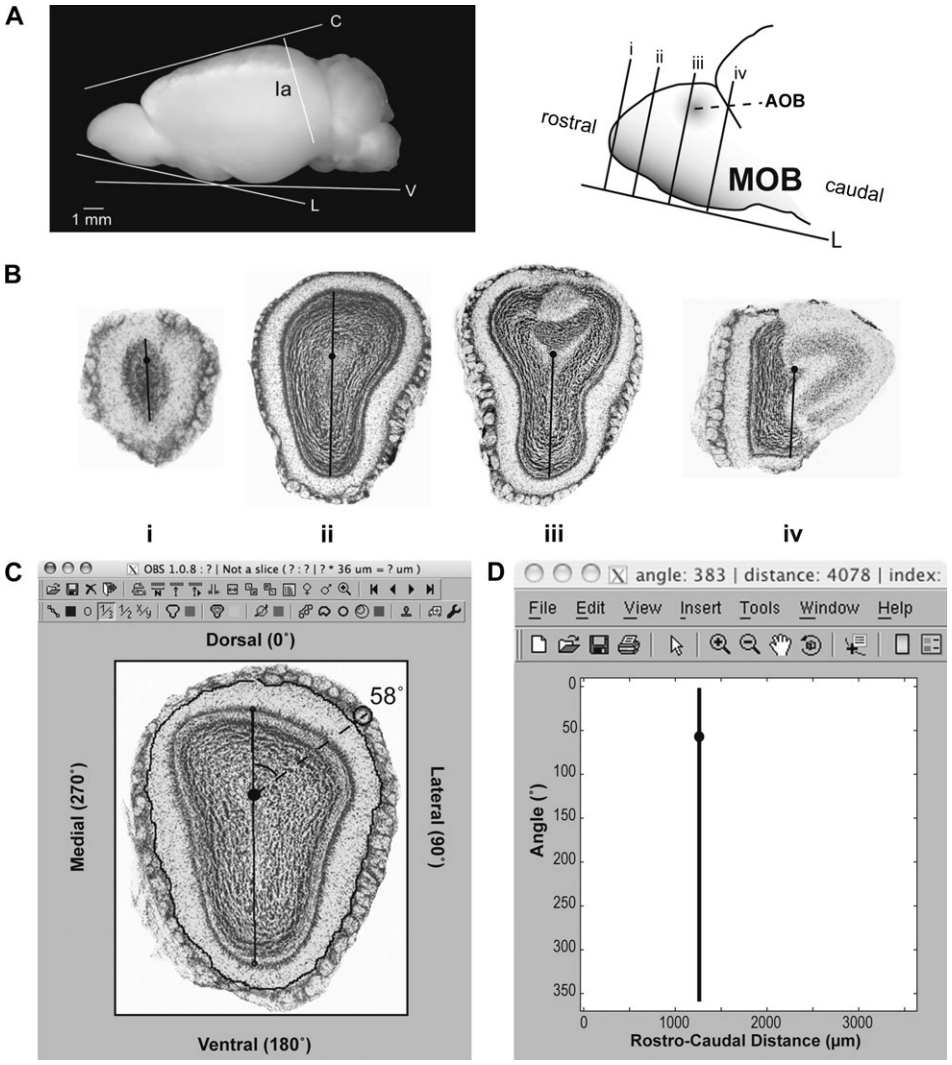

Figure 1 Mapping Method. **(A)** Lateral view of the mouse brain. Line L labels the plane parallel to the lateral olfactory tract along which the rostral–caudal distance is measured, whereas lines V and C label the planes parallel to ventral and dorsal surfaces of brain, respectively. Line Ia labels an approximation of the interaural line, as defined by Franklin and Paxinos (1997). The illustration depicts an enlarged sagittal view of the olfactory bulb. The four labeled lines on the cartoon (i–iv) indicate the approximate rostro–caudal location of the sections shown in B. **(B)** Sequential transverse sections from an olfactory bulb cut perpendicular to the lateral olfactory tract as depicted in the cartoon in A. The black line on each section indicates the orientation of the 0°–180° axis, and the dot on the line indicates the location of the origin. (i) Rostral landmark. (iii) AOB landmark. **(C, D)** Screen shots from GLOM•MAP *OBS*. (C) A digital image loaded into OBS, with origin, perimeter, and glomerulus in black. **(D)** Scatterplot of the mapping information acquired in C. The cylindrical coordinates of the stamped glomerulus is approximately 58° and 789° µm. Panel A was reproduced with permission from Schaefer *et al.* (2001a).

capable of transforming the data into a 2-D density map or a 3-D surface representation of the 2-D density map. The software includes several algorithms to compare multiple 2-D maps. While our mapping technique was developed for the murine bulb sectioned perpendicular to the L plane (see Figure 1A), our software can easily handle images cut in other planes or from other species. In fact, the software has been used to map glomeruli in such species as the sea lamprey (B. Zielinkski, personal communication) and ferret (Woodley *et al.*, 2004). For bulbs sectioned in alternate planes, the user will have to establish reliable anatomical landmarks to orient the cylindrical coordinate axis in each section. To map a single bulb using our software typically requires several hours. Our software is available for download on the Restrepo laboratory Web site (http://www.uchsc.edu/rmtsc/restrepo/, under ''Biomedical Info and TOOLS'').

Glomerular analysis

Glomerular Analysis 2.0 (GlomA), a plugin for ImageJ, provides all the functionality of Glomerular Analysis 1.0, which we first introduced in 2001 (Schaefer *et al.*, 2001a). This plugin includes the basic tools necessary to map glomeruli in the olfactory bulb as described in Mapping Technique. GlomA allows users to open a digital image of an olfactory bulb section, enter the rostro–caudal position of the section,

and draw a dorsoventral axis line. Once this axis is set, a user then traces the glomerulus of interest on the digital image using the built-in drawing tools of ImageJ. The software records the cylindrical coordinates of the glomerulus along with such information as the cross-sectional area of the glomerulus and mean intensity of the pixels inside the selection. The plugin provides immediate visual feedback for the user by plotting the cylindrical coordinates of stamped glomeruli on a 2-D scatterplot. Mapped data are saved as a text file.

GlomA offers the following improvements over its previous version. (1) Multiple methods to set the origin, accommodating the technique detailed in Mapping Technique and an alternate technique detailed by the Johnson *et al.* method (Johnson *et al.*, 1999). (2) The ability to draw and calibrate a glomerular perimeter. Once a glomerular perimeter has been manually traced and calibrated, our software records both geometric and cylindrical coordinates of a glomerulus. (3) Additional information recorded when a glomerulus is stamped, including the distance of the stamped glomeruli along the glomerular perimeter and RGB pixel intensity information. (4) More flexible 2-D map display options. (5) ''Group ID'' designation (an integer number), facilitating the statistical comparison of different data sets using our data analysis software, GLOM•MAP *GDB*. (6) An ''UNDO'' button, which removes the recorded information from the last glomerular stamp. (7) The ability to mark damaged areas in a particular section (''Stamp Gap''), which is important for statistical analysis of the data (see Transformation and Analysis Software).

GLOM•MAP OBS

We have recently transferred the capabilities of GlomA into the MATLAB development environment. MathWorks products have been widely adopted in the academic community for teaching and research in a broad range of technical disciplines (The MathWorks, Inc.). By rewriting the GlomA code into the MATLAB programming language, we have accelerated our developmental cycle, facilitated customization, improved the mapping capabilities, and increased the user-friendliness of the software. We call this new software module GLOM•MAP *OBS* (OBS) (Figure 1C,D).

In addition to the capabilities provided by GlomA, OBS allows for text designation of Group ID (e.g., ''control''), making database management less confusing and more user-friendly (see Transformation and Analysis Software). Users can also indicate the sex of the animal being mapped. The index of a section can easily be changed, or all indices can be offset if further analysis indicates that the anatomical landmarks were initially set incorrectly. Moreover, the mapping tools have been vastly improved. The origin can now be set anywhere along the axis line, allowing a user to customize the location of the origin. There is a ''multi-stamp'' tool, which allows a user to quickly and repeatedly stamp glomeruli of a predesignated size with a click of the mouse. Marking damaged areas of a tissue section is simpler and more intuitive. A user can now set the color of each mapping object to better contrast the tissue labeling method employed or to color-label objects for more complex data sets. Also, any mapping object (e.g., axis line or glomerular trace) placed on a digitized section can be moved or deleted at any time, and the changes will be reflected immediately in the data file. In addition, OBS includes a navigable scatterplot (Figure 1D): a simple click on a data point brings up the digital image of the referenced section and the associated mapping objects. The program also includes export capabilities that allow a user to save scatterplots as images in industry standard formats such as Encapsulated PostScript, Adobe Illustrator, Tagged image file format, and Portable document format.

Transformation and analysis software

The new GLOM•MAP *GDB* (GDB) module combines the functionality of our discontinued transformation and analysis software, To•Matrix (Schaefer *et al.*, 2001b), with a graphical user interface (GUI). GDB also adds plotting capabilities and new statistical functions. GDB has two windows: a data set manager window and a data viewer window (Figure 2). Using the data set manager, a user can rapidly import multiple raw data files generated in either GlomA or OBS (Figure 2B). These files are converted into a raw data set file that can be read by GDB and then sorted, based on Group ID (see mapping software), into a directory-based database that draws on the strength and flexibility of the host operating system. After import, each data set file can be added to the data set manager either individually or en masse based on the Group ID of each data set. Once added to the data set manager, GDB functions, such as generating a binned activation map, can be run simultaneously, greatly accelerating the work flow. Alternatively, a user can export the data to an Excel (Microsoft, Inc., Redmond, WA) spreadsheet and analyze the data from there.

To generate each activation map, the software performs a histogram count on the raw data, grouping the positive glomerular counts into bins of 10° (or 1/36 the maximum perimeter length) and 72 μm. Bins that do not have a value—e.g., bins in areas of the sample where the tissue was marked ''damaged'' (and subsequently not mapped)—are assigned the value ''NaN'' (not-a-number). Once the data files are transformed, the activation maps are plotted as 2-D density plots (Figure 3A–C). For each plot, the cylindrical coordinates of each bin are plotted along the x and y axes, while the color of the bin represents the bin value. GDB provides many controls to display the data, including a standardized 2-D plot view or a statistical log view. NaN and false discovery rate (FDR) outlines can be added or removed, as required. GDB can also plot activity maps in 3-D and can add glomeruli to this 3-D view as shown in Figure 6. Note that while these 3-D plots are useful, they should be used for visualization purposes only and should not be used to infer any statistical conclusions. Also note that the anterior portion of the bulb will be added in a future version of the software. Once displayed, all plots can

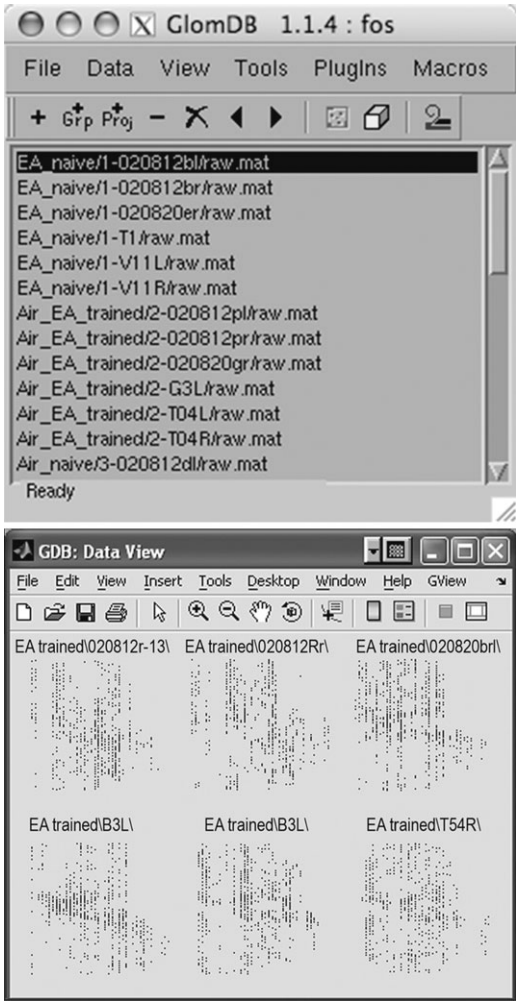

Figure 2 Screenshots from the GLOM•MAP *GDB* data analysis software module demonstrating the ease in generating odor maps. Upper panel: The GDB data set manager listing raw files from the EA project. The data set manager has a toolbar for commonly used commands and menus for the rest of the commands. The plugins menu can accommodate add-on functions written in the MATLAB programming language. Lower panel: The GDB Data View window plotting six files from the EA-trained group. The GView Menu has commands for changing the properties of the plots.

be exported into a variety of industry-standard formats for the generation of publication-quality figures, such as those presented in Figures 3–6.

GDB offers several statistical functions to aid in the analysis of binned activation maps. In all the included statistical functions, bins assigned a value of NaN are excluded from the calculations. Users can select to "smooth" a map, which applies a 2-D convolution with a uniform 3×3 kernel to the highlighted data matrix in the file manager. Users can also "normalize" the data files which divides the data matrices for all files loaded in the file manager by the matrix of the highlighted file, or they can chose to "average" the data files, which averages the data binwise across all the data matrices. Finally, users can choose to run a point-by-point Mann–Whitney *U* test, provided files from at least two different groups (Group ID) are loaded in the file manager. The Mann–Whitney function calculates the probability that the median for bin values at the same cylindrical coordinates across all the matrix files is different between the two groups. Similar to the procedure described in Schaefer *et al.* (2001b), the function calculates a *P* value for each bin by sorting an estimation of *U* for all the values in the bin and the encompassing eight bins surrounding it across all the files being compared. The function labels the *P* value as significant when it falls below a critical value determined by the FDR procedure that corrects for the large number of multiple comparisons performed when every pixel in an image is compared (Curran-Everett, 2000). Once the calculations are complete, the function plots the statistical difference between each group as a single, 2-D matrix populated with *P* values (Figure 3D). Since GDB is presented as an open-source software package, all the included statistical functions can easily be modified with a nominal understanding of the MATLAB programming language.

GDB plugins

GDB offers the user the option of adding "plugins" with user-defined statistical and plotting functions not included in the GDB tool set. A template is provided to allow users to create their own plugins for GDB using the MATLAB programming language. We have generated two plugins (gProcess and gBrowser) for the collection of statistical information from labeled glomeruli, such as the P2 and M72 glomeruli, that were labeled with the genetic tau-LacZ marker (Mombaerts *et al.*, 1996; Zheng *et al.*, 2000). gProcess is an add-on tool that allows a user to manually collate the cross-sections from a single glomerulus across multiple cryosections. Once collated, the tool can then extract from these cross-sections statistical information, such as the median distance, angle, area, approximate volume, and length for the selected glomerulus. The information for each glomerulus generated in this fashion can be saved as a new, processed data file with each data point representing the entire glomerulus. M72 and P2 glomeruli processed in this fashion are displayed in Figure 6, as yellow and green ovoids, respectively. Another add-on tool, gBrowser, can open multiple processed data files and calculate from these files the mean anteroposterior location, volume, or any selectable metric of glomeruli from a particular region of the bulb, such as the rostrolateral or caudomedial region.

Generation of histograms of *c-fos*–positive counts per bin

In order to generate the histograms of *c-fos*–positive counts per bin as shown in Figure 4, we grouped binwise by mean *c-fos*–positive counts across an experimental group (e.g., the group of trained mice). We grouped all the counts in bins from different animals that had the same cylindrical coordinates as an averaged bin (Figure 4A,B) with a mean count that fell between $x - \delta$ and $x + \delta$ (where δ was 0.3 and x was the mean count). Thus, for a mean count of 1 ($x = 1$), we included all counts from bins located in the same locations

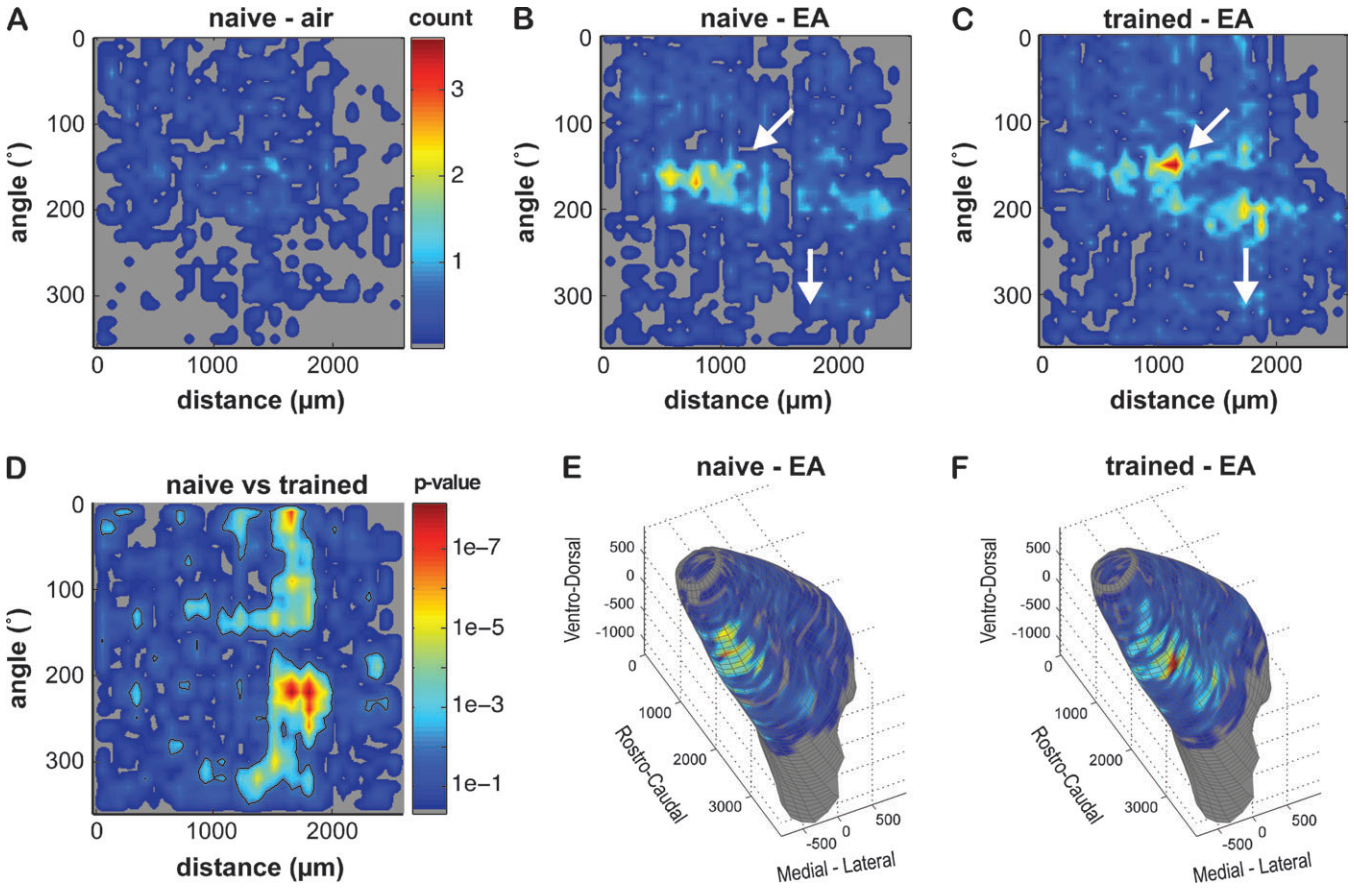

Figure 3 **(A–C)** Averaged density odor maps from naïve, air-exposed mice (n = 6); naïve, EA-exposed mice (n = 5); and trained, EA-exposed mice (n = 6), respectively. In each odor map, each averaged bin is plotted according to its cylindrical coordinates: angle versus rostral–caudal distance from the anterior landmark. The color of each bin indicates its average histogram count and ranges from 0 to up 3.6 (in the trained map). Gray indicates regions of the bulb that did not contain any active glomeruli. The white arrows indicate the corresponding regions in each map. **(D)** Mann–Whitney P value map. Five EA odor maps from the naïve animals were compared to six EA odor maps from the trained animals. Each bin has a P value corresponding to the probability that summed bin counts from the naïve group are different than the counts from the trained group. As in A–C, bins are plotted according to their cylindrical coordinates. The color of each bin corresponds to its P value, with bluer colors indicating less significance and the redder colors indicating more significance. The black outlines enclose the FDR determined regions of significance. **(E, F)** 3-D representations of the odor maps plotted in B and C oriented so that the rostral aspect of the bulb projects out of the page diagonally to the left, dorsal aspect is on the top, and the lateral aspect projects out of the page diagonally to the right.

as the averaged bins that had a mean between 0.7 and 1.3 (Figure 4A, blue squares). In order to generate the histogram for Figure 4C, a bin of 10 × 72 μm was used, while for the histogram in Figure 4D, larger bins of 30 × 72 × 3 μm were used. The histograms were fit with a Poisson distribution using the nonlinear least squares fit function of MATLAB.

Results

The number of EA-induced *c-fos*–positive glomeruli is larger in trained mice compared to naïve mice

We used GlomA to map *c-fos* activity in response to EA exposure in the olfactory bulbs of two groups of animals (trained and naïve). As shown in Figure 3, the odor maps indicated a robust up-regulation of glomerular activation for animals that had previously been trained to detect EA as compared to animals exposed to air. For the trained animals, the average number of glomeruli activated was 540 with a SD of 55 (n = 6); for naïve animals, the mean number of activated glomeruli was significantly smaller (tested with an analysis of variance with a *Post hoc* Tukey's test, $P < 0.05$): 401 ± 129 trained (n = 5). By comparison, regardless of pretreatment, control animals exposed to air had an average number of activated glomeruli that was less than half the number of glomeruli activated in EA-exposed groups (189 ± 58 for trained animals and 190 ± 71 for naïve animals). This background signal upon exposure to fresh air is due to detection of "self" odor (urine, feces, and other secretions).

The training-induced changes in glomerular activity are spatially restricted to circumscribed regions of the glomerular sheet

Shown in Figure 3A–C are averaged, smoothed odor maps generated from naïve animals exposed to air and the trained

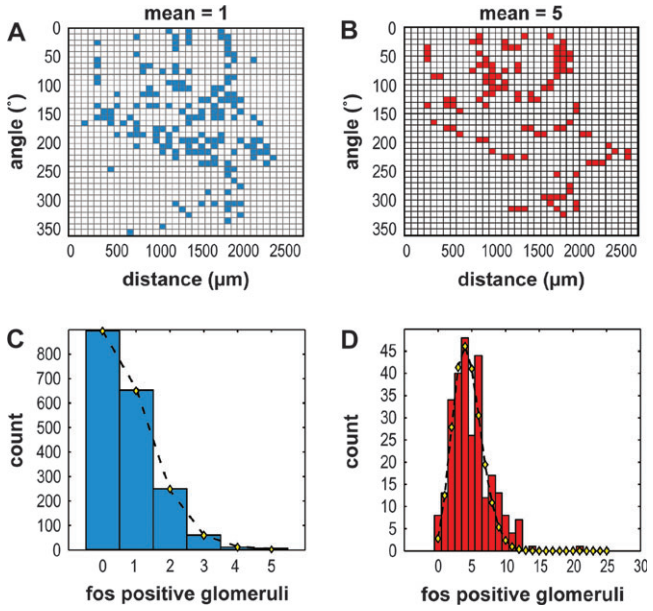

Figure 4 Histograms of *c-fos*–positive counts have a Poisson distribution. Details for generating these histograms can be found in Methods. **(A)** Average of all *c-fos* density plots from EA-trained animals. Blue squares indicate bins that had an average *c-fos*–positive count falling between 0.7 and 1.3. **(B)** Smoothed average of *c-fos* density plots from all EA-trained animals. Red squares indicate bins with an average count of between 4.7 and 5.3. **(C)** A histogram of the counts from the bins in each individual density plot corresponding to the blue bins in the averaged plot. **(D)** A histogram of the counts from the bins in each individual density plot corresponding to the red bins in the smoothed, averaged plot. Yellow diamonds: least squares fit of the Poisson distribution.

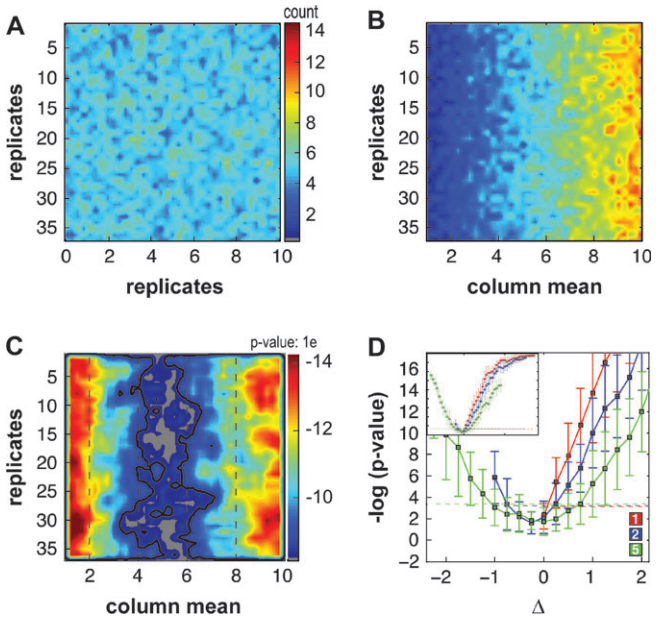

Figure 5 Simulated activity maps. **(A)** A flat map populated with Poisson-distributed random numbers across both rows and columns with a sample mean μ of 5. The color bar is mapped to the range of counts found across bins in (A) and **(B)**, with 1 count mapped to blue and >14 counts mapped to red. (B) A ramp map populated with Poisson-distributed random numbers where the sample means μ increase incrementally across columns from 1 to 10. **(C)** Mann–Whitney *P* value map from a comparison of six ramp maps with six flat maps that have a sample mean μ of 5 (as shown in A). The solid black outlines enclose regions of significance determined by the FDR. **(D)** *P* values as a function of the difference between mean counts (Δ). Because *P* values change by orders of magnitude, the negative of the logarithm of the *P* value is shown in the vertical axis. Δ = the difference between the mean count per bin (μ) used in the generation of Poisson-distributed numbers in the columns of the ramps ("column means") minus the mean of counts per bin (μ) in the flat map (varied from 1 to 5). Red = ramp maps compared to flat maps with a count per bin mean of 1. Blue = ramp maps versus flat maps with a mean of 2. Green = ramp map versus flat maps with a mean of 5. The dashed horizontal lines are the FDR cut-off values. Negative log *P* values above the FDR cut-off line are considered significant. Inset: expanded horizontal axis.

and naïve animals exposed to EA. Although plotted using different coordinates, the EA activity map in the naïve animals appears to correlate well with the EA activity maps detected in mice using fMRI (Xu *et al.*, 2003). At a glance, the map from the naïve animals displays some dissimilarity to the map from the trained animals. The trained animals appear to have a pair of intense activation peaks and an area of medial activity (Figure 3C and F, white arrows), whereas the corresponding peak in the naïve animals is less intense and more diffuse and the medial activity is less extensive (Figure 3B and E: see arrows). To determine the statistical significance of this dissimilarity, we ran a point-by-point Mann–Whitney test with false discovery correction on the density files from the two groups. As shown in Figure 3D, there is a significant region of dissimilarity in the caudal region of the bulb, particularly between 1,200 and 2,000 μm.

Counts of *c-fos*–positive glomeruli within each bin in the odor map follow Poisson statistics

In order to better understand the nature of the variance within *c-fos* odor maps, we sought to understand the statistical distribution of counts of *c-fos*–positive glomeruli within each bin of the odor map. Shown in Figure 4 are the histograms (bar graphs) of *c-fos*–positive glomeruli within bins across trained group activity maps that had a mean count of either 1 (Figure 4A) or 5 (Figure 4B) (see Methods for details on how these histograms were generated). As depicted by the dashed line and yellow diamonds, these counts are proportional to a Poisson probability distribution

$$P = e^{-\mu}\mu^{k}/k!,$$

where P is the probability for a given k, μ is the mean count, and k is the number of counts per bin. We found a similar distribution for other values of mean count (μ) as well as in the activity maps from the naïve animals and in odor maps of a previously published study of urine-elicited odor activity maps (Schaefer *et al.*, 2001b) (data not shown), indicating that activation of *c-fos* in the glomerular layer of the olfactory bulb follows a Poisson distribution.

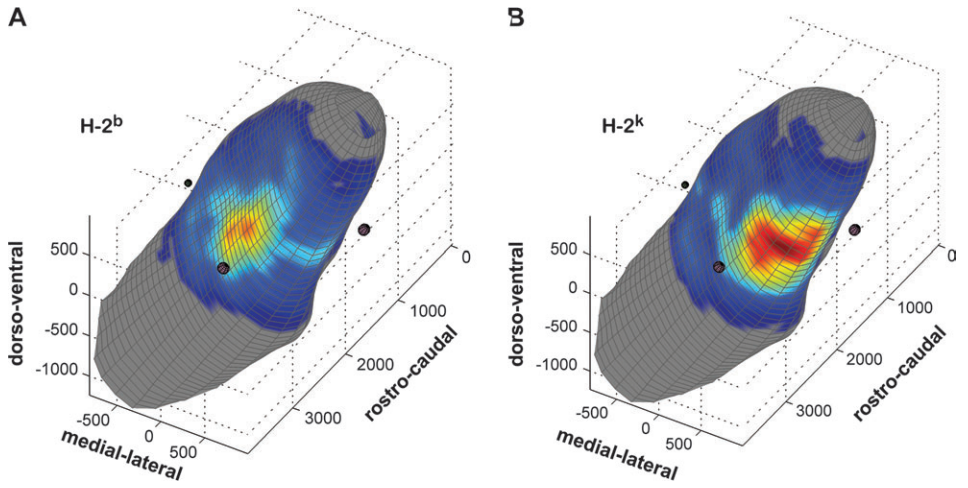

Figure 6 3-D view of *c-fos* activity elicited from H-2^b **(A)** and H-2^k **(B)** urines in a female mouse [these data were taken from data previously published by our group, Schaefer *et al.* (2001b); copyright 2001 by the Society for Neuroscience] (Schaefer *et al.*, 2001b). For the surface maps, the color scales are similar to those in Figure 3. Mapped and processed glomeruli from the P2iTLZ mice (pink oviods) and the M72iTLZ mice (green ovoids) have been added to the 3-D views to serve as fiduciary markers. Notice the asymmetrical activity in the H-2^b response as compared to the H-2^k response.

Validation of the Mann–Whitney statistical test used to determine significance of differences between odor maps

To validate the Mann–Whitney test for determining the statistical significance of differences in odor maps, we generated multiple, simulated activity maps, exploiting the fact that counts of *c-fos*–positive glomeruli vary according to Poisson statistics (see Figure 5). We generated two types of 37×37 simulated map matrices: a "flat" map and a "ramp" map. Each flat matrix was filled with random Poisson-distributed numbers with sample means of 1, 2, or 5 across the entire matrix (in concordance with typical per bin values found in our measured odor maps). Figure 5A shows a flat matrix with a mean value of 5. Each ramp matrix (Figure 5B) was filled with random Poisson-distributed numbers distributed across the matrix rows with sample means that incrementally increased across the matrix columns from 1 to 10. We used the GDB Mann–Whitney function to compare six independently generated flat matrices with six ramp matrices. The Mann–Whitney calculated two large regions of significance between column means 1–4 and 6–10 in the ramp matrix, with a single large region lacking statistical significance centered around ramp column means 4–6 (Figure 5C). As expected, the region with a mean between 4 and 6 in the ramp matrix is not significantly different because it is being compared with a flat matrix with a mean of 5. Similar results were seen in the comparison of the ramp maps to flat maps with sample means of 1 and 2 (not shown). For each Mann–Whitney P value matrix, we calculated an average P value for the replicates across rows in the same column. Figure 5D shows the negative logarithm of these P values plotted as a function of the difference (Δ) between the column mean of the ramp matrices (1–10) and the mean value for the flat matrices (1, 2, or 5). The horizontal dotted lines indicate the FDR cut-off for significance. P values that fall below these lines are not considered significantly different from control, while values above the lines are considered to be significantly different. Importantly, the P value fell substantially below FDR when the mean value for the counts were both 5, ensuring that our statistical test rarely rejects a true null hypothesis (i.e., finds that the two samples have different means when in fact they have the same mean; also known as a Type I or false alarm error).

Discussion

In this article, we have demonstrated the effects that intensive behavioral training can have on odorant-induced activity in the glomerular layer of the olfactory bulb. Using *c-fos* up-regulation as a marker of glomerular activity, we tracked the responsiveness of the glomerular layer to EA in mice trained by go/no-go operant conditioning task of Bodyak and Slotnick (1999) and in naïve mice. We analyzed the data using a new suite of computational tools suitable for mapping and performing statistical comparisons of odor-induced activity in the glomerular layer of the olfactory bulb. We showed that the EA odor maps of the trained and naïve animals have differences that are statistically significant. In addition, we showed that counts of *c-fos*–positive glomeruli per bin in our odor maps follow Poisson statistics. This allowed us to perform a validation of the Mann–Whitney statistical test of differences among *c-fos* odor maps used in our computational suite.

Methods for mapping activity in the olfactory bulb

A more comprehensive understanding of the molecular basis of odor activity maps requires the reproducible mapping of functional and molecular features in the glomerular layer of the olfactory bulb. Our software facilitates mapping using

the method developed by our group for the mouse olfactory bulb (Schaeffer *et al.*, 2001a,b) based on the method formulated by Johnson *et al.* (1999) to map 2-DG activity maps in rats (Johnson and Leon, 1996). A related mapping tool (OdorMapBuilder) was recently generated by Liu and coworkers to allow mapping of odor maps measured in fMRI studies (Liu *et al.*, 2004). The open-source software presented here allows reproducible mapping of molecularly tagged glomeruli or glomerular activity. Because our method yields maps that can be compared from animal to animal, the maps can be stored in a database and incrementally added to a global functional–molecular odor map. This powerful computational tool will facilitate a thorough understanding of the molecular basis for information content in odor maps. Our software consists of GlomA and GLOM•MAP. GlomA is an updated plugin (Schaefer *et al.*, 2001a) for the National Institutes of Health–sponsored image-processing program (ImageJ) that can be used to map glomeruli. GLOM•MAP is a self-contained mapping and analysis tool that includes two toolboxes written in the MATLAB development environment. The GLOM•MAP *OBS* toolbox includes the functionality of GlomA plus many improvements, whereas GLOM•MAP *GDB* is our new data analysis toolbox, which overhauls the functionality of To•Matrix (Schaefer *et al.*, 2001b) and provides some new GUI elements that greatly simplify and accelerate the work flow.

Comparison with published EA odor maps

We used our software to determine potential differences between odor maps for two groups of mice: mice trained to discriminate EA in an olfactometer and mice that were not. After the training period, we exposed both groups of mice to EA and then recorded the glomerular activity pattern using GlomA. Using GDB to generate 2-D odor maps, we compared our maps to EA maps generated in other laboratories using different techniques and different species of animals. Interestingly, the EA activity maps detected by *c-fos* in naïve mice appear to correspond nicely with the EA activity maps detected in anesthetized mice by fMRI (Xu *et al.*, 2005), but appear to differ from the EA maps detected by 2-DG in rats (http://leonlab.bio.uci.edu/), which lack significant activity in the ventral region of the bulb. While it may be argued that the different detection methodologies could have introduced conflicting mapping artifacts, the odor maps from odorants such as aliphatic alcohols, acids, and ketones appear to have good agreement between mice and rat as found in a comparison of fMRI and IEG expression odor maps in mouse (Inaki *et al.*, 2002; Xu *et al.*, 2005) with those of Michael Leon and Bret Johnson in rat (http://leonlab.bio.uci.edu/). Thus, the fact that the EA odor maps from mice and rats appear to differ suggests a species-specific difference in the distribution of odorant-induced activity in the ventral areas of the glomerular layer of the olfactory bulb. Clearly, further work is necessary to investigate this potential difference between species. A particularly intriguing possibility is that in mice the ventral area of the olfactory bulb might be specialized in responding to socially relevant odors. In support of this contention, we have found that putative pheromones elicit activity in the ventral area of the olfactory bulb in mice defective for subunit A2 of the cyclic nucleotide-gated channel (Lin *et al.*, 2004). We also have evidence showing that the population of OSNs targeting the ventral region of murine bulb expresses unique transduction components such as the transient receptor potential m5 ion channel (Lin *et al.*, 2005).

c-fos–positive counts follow Poisson statistics

To study the nature of the variability in our odor maps, we calculated the distribution of *c-fos*–positive counts per bin and discovered that they follow a Poisson distribution (Figure 4A,B). The Poisson distribution has been used to describe a wide range of biological phenomena and may have important implications for our data. For example, these data support the contention that from mouse to mouse, glomeruli become *c-fos*–positive in a probabilistic all or none fashion, providing further evidence that the glomeruli themselves are activated in an all or none fashion (Xu *et al.*, 2000a). The fact that histograms of *c-fos*–positive counts had a distribution proportional to the Poisson distribution allowed us to validate the use of the Mann–Whitney *U* statistical test for comparing odor maps. Our results indicate that this test is suitable for determining the statistical significance of differences in *c-fos*–positive counts throughout the glomerular layer.

Training induces changes in EA odor maps

We analyzed the EA odor maps using a point-by-point Mann–Whitney *U* test statistical function. From this analysis, we discovered several statistically significant regions of variability in the odor maps between the two groups, suggesting a change at the cellular level that coincides with olfactometer training. In these experiments, we are measuring *c-fos* expression in juxtaglomerular cells. Because activity in these cells is affected not only by input from the OSNs, but also by feedback from other juxtaglomerular cells as well as mitral cells (Wilson *et al.*, 1996; Schoppa *et al.*, 1998; Shepherd *et al.*, 2004), this change in the *c-fos* activity maps likely reflect a change in signal processing elicited in the olfactory bulb by training in the Bodyak and Slotnick olfactometer. However, the changes could also reflect peripheral changes in OSN populations (Watt *et al.*, 2004). Further experiments are necessary to determine the causes of training-induced changes in odor signal processing.

Our computational tools allow relating odor maps to molecular maps in the glomerular layer

Perhaps the most significant contribution of our software will be to facilitate the systematic development of a database

that relates functional to molecular features. We demonstrate this potential by relating urine odor activity maps to the location of molecularly tagged glomeruli (Figure 6). While it is clear that molecularly identified glomeruli are arranged in two mirror maps in the glomerular layer, the axis of symmetry of this arrangement is not related in a simple manner to anatomical features in the bulb. However, the axis of symmetry can be revealed by relating functional maps to molecular maps. Indeed, Inaki and coworkers have studied odor maps in mouse and related them to molecular feature maps set by patterns of expression of the Rb8 neural cell adhesion molecule (RNCAM/OCAM) and neuropilin-1, which are preferentially expressed in circumscribed areas in the glomerular layer in the olfactory bulb (Inaki *et al.*, 2002). In this study, we illustrate the usefulness of our software by relating urine odor activity maps to identified glomeruli. In a previous study, we compared *c-fos* activation in a female olfactory bulb elicited by urine obtained from two different haplotypes of mice (Schaefer *et al.*, 2001b). The 2-D odor maps generated with GDB were identical to the maps we reported in Schaefer *et al.* (2001b, data not shown). Furthermore, a 3-D examination of these maps plotted with M72 and P2 glomeruli (Figure 6) highlights a curious feature of the maps: whereas the H-2^k map is fairly symmetrical along the ventral surface of the bulb, the H-2^b map is shifted asymmetrically towards the ventro-medial surface. This shift is surprising considering that the typical response to a single chemical feature has been demonstrated to be symmetrical (Johnson *et al.*, 1999; Inaki *et al.*, 2002) and suggests that the response elicited from a complex odor may be more complicated than a simple summation of its individual components. Because these odor maps were determined by *c-fos* up-regulation, which is a measure that could be influenced by interglomerular as well as intraglomerular processing, the asymmetry in the odor maps may be due to mirror differences in local processing of the signal. Alternatively, the asymmetry may be due to differences in accessibility of the odorants to the OSNs innervating the two mirror glomerular maps. The asymmetry of the H-2^b map becomes evident when related to the molecularly labeled glomeruli in the 3-D view, highlighting the importance of visualizing the data in both 2-D and 3-D.

Our software provides a comprehensive means to map and examine, at a single glomerular resolution, odor-induced glomerular activity and molecular features of glomeruli throughout the olfactory bulb. We have added tools to greatly simplify and accelerate the work flow. While our current mapping software can be used to consistently map glomeruli from a bulb cut in a specific plane, it is limited by the need to have well-defined anatomical landmarks for the orientation of each section. To overcome this obstacle, we intend to develop a more universal mapping technique that will allow a user to fit sections cut from any plane of the bulb into a standard bulb and thus eliminate the need for any one specific mapping technique. We hope to release in a future version of our software such a standard bulb, which would serve as a model onto which various molecular or functional features could be mapped. The overlay of such features on a model bulb could provide further insights into the underlying molecular basis of odor maps and could serve as a reference point for future investigation. Additionally, the comparison of these odor maps with the maps generated using alternative techniques should further enrich our understanding of odorant coding in general.

Acknowledgements

We would like to thank Robin L. Michaels for her insightful review of the manuscript and anonymous reviewers for thoughtful criticisms that motivated the Poisson distribution analysis. This project was supported by National Institutes of Health grants DC00566, DC04657, DC006070, and MH068582.

References

Bodyak, N. and **Slotnick, B.** (1999) *Performance of mice in an automated olfactometer: odor detection, discrimination and odor memory.* Chem. Senses, 24, 637–645.

Buck, L.B. (2000) *The molecular architecture of odor and pheromone sensing in mammals*. Cell, 100, 611–618.

Curran-Everett, D. (2000) *Multiple comparisons: philosophies and illustrations*. Am. J. Physiol. Regul. Integr. Comp. Physiol., 279, R1–R8.

Franklin, K.B.J. and **Paxinos, G.** (1997) The Mouse Brain in Stereotaxic Coordinates. Academic Press, San Diego, CA.

Friedrich, R.W. and **Korsching, S.I.** (1998) *Chemotopic, combinatorial, and noncombinatorial odorant representations in the olfactory bulb revealed using a voltage-sensitive axon tracer.* J. Neurosci., 18, 9977–9988.

Guthrie, K.M., Anderson, A.J., Leon, M. and **Gall, C.** (1993) *Odor-induced increases in c-fos mRNA expression reveal an anatomical "unit" for odor processing in olfactory bulb*. Proc. Natl Acad. Sci. USA, 90, 3329–3333.

Inaki, K., Takahashi, Y.K., Nagayama, S. and **Mori, K.** (2002) *Molecular-feature domains with posterodorsal-anteroventral polarity in the symmetrical sensory maps of the mouse olfactory bulb: mapping of odourant-induced Zif268 expression*. Eur. J. Neurosci., 15, 1563–1574.

Johnson, B.A. and **Leon, M.** (1996) *Spatial distribution of [14C]2-deoxyglucose uptake in the glomerular layer of the rat olfactory bulb following early odor preference learning*. J. Comp. Neurol., 376, 557–566.

Johnson, B.A. and **Leon, M.** (2000a) *Modular representations of odorants in the glomerular layer of the rat olfactory bulb and the effects of stimulus concentration*. J. Comp. Neurol., 422, 496–509.

Johnson, B.A. and **Leon, M.** (2000b) *Odorant molecular length: one aspect of the olfactory code*. J. Comp. Neurol., 426, 330–338.

Johnson, B.A., Woo, C.C., Duong, H., Nguyen, V. and **Leon, M.** (1995) *A learned odor evokes an enhanced Fos-like glomerular response in the olfactory bulb of young rats*. Brain Res., 699, 192–200.

Johnson, B.A., Woo, C.C., Hingco, E.E., Pham, K.L. and **Leon, M.** (1999) *Multidimensional chemotopic responses to n-aliphatic acid odorants in the rat olfactory bulb*. J. Comp. Neurol., 409, 529–548.

Lin, W., Arellano, J., Slotnick, B. and **Restrepo, D.** (2004) *Odors detected by mice deficient in cyclic nucleotide-gated channel subunit A2 stimulate the main olfactory system*. J. Neurosci., 24, 3703–3710.

Lin, W., Margolskee, R.F., Zhao, Z., Liman, E.R. and **Restrepo, D.** (2005) *Expression of TRPM5 in the main olfactory epithelium [abstract]*. Chem. Senses, 30, A127.

Liu, N., Xu, F., Marenco, L., Hyder, F., Miller, P. and **Shepherd, G.M.** (2004) *Informatics approaches to functional MRI odor mapping of the rodent olfactory bulb: OdorMapBuilder and OdorMapDB*. Neuroinformatics, 2, 3–18.

Mombaerts, P., Wang, F., Dulac, C., Chao, S.K., Nemes, A., Mendelsohn, M., Edmondson, J. and **Axel, R.** (1996) *Visualizing an olfactory sensory map*. Cell, 87, 675–686.

Montag-Sallaz, M. and **Buonviso, N.** (2002) *Altered odor-induced expression of c-fos and arg 3.1 immediate early genes in the olfactory system after familiarization with an odor*. J. Neurobiol., 52, 61–72.

Munger, S.D., Lane, A.P., Zhong, H., Leinders-Zufall, T., Yau, K.-W., Zufall, F. and **Reed, R.R.** (2001) *Central role of the CNGA4 channel subunit in Ca2+-calmodulin-dependent odor adaptation*. Science, 294, 2172–2175.

Nagao, H., Yoshihara, Y., Mitsui, S., Fujisawa, H. and **Mori, K.** (2000) *Two mirror-image sensory maps with domain organization in the mouse main olfactory bulb*. Neuroreport, 11, 3023–3027.

Ressler, K.J., Sullivan, S.L. and **Buck, L.B.** (1994) *Information coding in the olfactory system: evidence for a stereotyped and highly organized epitope map in the olfactory bulb*. Cell, 79, 1245–1255.

Royet, J.P., Sicard, G., Souchier, C. and **Jourdan, F.** (1987) *Specificity of spatial patterns of glomerular activation in the mouse olfactory bulb: computer-assisted image analysis of 2-deoxyglucose autoradiograms*. Brain Res., 417, 1–11.

Rubin, B.D. and **Katz, L.C.** (1999) *Optical imaging of odorant representations in the mammalian olfactory bulb*. Neuron, 23, 499–511.

Sallaz, M. and **Jourdan, F.** (1993) *C-fos expression and 2-deoxyglucose uptake in the olfactory bulb of odour-stimulated awake rats*. Neuroreport, 4, 55–58.

Schaefer, M.L., Finger, T.E. and **Restrepo, D.** (2001a) *Variability of position of the P2 glomerulus within a map of the mouse olfactory bulb*. J. Comp. Neurol., 436, 351–362.

Schaefer, M.L., Young, D.A. and **Restrepo, D.** (2001b) *Olfactory fingerprints for major histocompatibility complex-determined body odors*. J. Neurosci., 21, 2481–2487.

Schoppa, N.E., Kinzie, J.M., Sahara, Y., Segerson, T.P. and **Westbrook, G.L.** (1998) *Dendrodendritic inhibition in the olfactory bulb is driven by NMDA receptors*. J. Neurosci., 18, 6790–6802.

Sharp, F.R., Kauer, J.S. and **Shepherd, G.M.** (1977) *Laminar analysis of 2-deoxyglucose uptake in olfactory bulb and olfactory cortex of rabbit and rat*. J. Neurophysiol., 40, 800–813.

Shepherd, G.M., Chen, W.R. and **Greer, C.A.** (2004) *Olfactory bulb*. In Shepherd, G.M. (ed.), The Synaptic Organization of the Brain. Oxford University Press, New York, pp. 159–204.

Slotnick, B. and **Bodyak, N.** (2002) *Odor discrimination and odor quality perception in rats with disruption of connections between the olfactory epithelium and olfactory bulbs*. J. Neurosci., 22, 4205–4216.

Strotmann, J., Conzelmann, S., Beck, A., Feinstein, P., Breer, H. and **Mombaerts, P.** (2000) *Local permutations in the glomerular array of the mouse olfactory bulb*. J. Neurosci., 20, 6927–6938.

Uchida, N., Takahashi, Y.K., Tanifuji, M. and **Mori, K.** (2000) *Odor maps in the mammalian olfactory bulb: domain organization and odorant structural features*. Nat. Neurosci., 3, 1035–1043.

Vassar, R., Ngai, J. and **Axel, R.** (1993) *Spatial segregation of odorant receptor expression in the mammalian olfactory epithelium*. Cell, 74, 309–318.

Vedin, V., Slotnick, B. and **Berghard, A.** (2004) *Zonal ablation of the olfactory sensory neuroepithelium of the mouse: effects on odorant detection*. Eur. J. Neurosci., 20, 1858–1864.

Wachowiak, M. and **Cohen, L.B.** (2001) *Representation of odorants by receptor neuron input to the mouse olfactory bulb*. Neuron, 32, 723–735.

Watt, W.C., Sakano, H., Lee, Z.Y., Reusch, J.E., Trinh, K. and **Storm, D.R.** (2004) *Odorant stimulation enhances survival of olfactory sensory neurons via MAPK and CREB*. Neuron, 41, 955–967.

Wilson, D.A., Sullivan, R.M., Gall, C.M. and **Guthrie, K.M.** (1996) *NMDA-receptor modulation of lateral inhibition and c-fos expression in olfactory bulb*. Brain Res., 719, 62–71.

Woodley, S.K., Cloe, A.L., Waters, P. and **Baum, M.J.** (2004) *Effects of vomeronasal organ removal on olfactory sex discrimination and odor preferences of female ferrets*. Chem. Senses, 29, 659–669.

Xu, F., Greer, C.A. and **Shepherd, G.M.** (2000a) *Odor maps in the olfactory bulb*. J. Comp. Neurol., 422, 489–495.

Xu, F., Kida, I., Hyder, F. and **Shulman, R.G.** (2000b) *Assessment and discrimination of odor stimuli in rat olfactory bulb by dynamic functional MRI*. Proc. Natl Acad. Sci. USA, 97, 10601–10606.

Xu, F., Liu, N., Kida, I., Rothman, D.L., Hyder, F. and **Shepherd, G.M.** (2003) *Odor maps of aldehydes and esters revealed by functional MRI in the glomerular layer of the mouse olfactory bulb.* Proc. Natl. Acad. Sci. USA, 100, 11029–11034.

Xu, F., Schaefer, M., Kida, I., Schafer, J., Liu, N., Rothman, D.L., Hyder, F., Restrepo, D. and **Shepherd, G.M.** (2005) *Simultaneous activation of mouse main and accessory olfactory bulbs by odors or pheromones*. J. Comp. Neurol., 489, 491–500.

Zheng, C., Feinstein, P., Bozza, T., Rodriguez, I. and **Mombaerts, P.** (2000) *Peripheral olfactory projections are differentially affected in mice deficient in a cyclic nucleotide-gated channel subunit*. Neuron, 26, 81–91.

Accepted August 5, 2005